Incommensurate Charge Order Phase in Fe_2OBO_3 due to Geometrical Frustration

M. Angst,[1,*] R. P. Hermann,[2,3] W. Schweika,[2] J.-W. Kim,[4] P. Khalifah,[5,6] H. J. Xiang,[7] M.-H. Whangbo,[7] D.-H. Kim,[1]
B. C. Sales,[1] and D. Mandrus[1]

[1]*Materials Science and Technology Division, Oak Ridge National Laboratory, Oak Ridge, Tennessee 37831, USA*
[2]*Institut für Festkörperforschung, Forschungszentrum Jülich GmbH, D-52425 Jülich, Germany*
[3]*Department of Physics, B5, Université de Liège, B-4000 Sart-Tilman, Belgium*
[4]*Ames Laboratory, Ames, Iowa 50010, USA*
[5]*Department of Chemistry, University of Massachusetts, Amherst, Massachusetts 01003, USA*
[6]*Department of Chemistry, State University of New York, Stony Brook, New York 11794, USA*
[7]*Department of Chemistry, North Carolina State University, Raleigh, North Carolina 27695, USA*
(Received 20 July 2007; published 19 December 2007)

The temperature dependence of charge order in Fe_2OBO_3 was investigated by resistivity and differential scanning calorimetry measurements, Mössbauer spectroscopy, and synchrotron x-ray scattering, revealing an intermediate phase between room temperature and 340 K, characterized by coexisting mobile and immobile carriers, and by incommensurate superstructure modulations with temperature-dependent propagation vector $(\frac{1}{2}, 0, \tau)$. The incommensurate modulations arise from specific antiphase boundaries with low energy cost due to geometrical charge frustration.

Geometrical frustration, the inability of interactions to be simultaneously satisfied due to the geometry of the underlying crystal lattice, in the case of magnetic interactions is known to be responsible for incommensurate spin modulations [1] and for various exotic ground states [2]. The Coulomb interactions leading to charge order (CO) [3,4] can also be geometrically frustrated [5]. However, the effects of geometrical charge frustration are less well understood, despite the classical CO example [4] occurring on a frustrated lattice. Observations of incommensurate charge modulations are typically attributed to charge-density-wave-like Fermi-surface nesting scenarios [6,7], but unusually complex CO patterns observed in spinels [8], "devil's staircase"-type CO modulations found in NaV_2O_5 under pressure [9], and the appearance of a new type of ferroelectricity upon charge ordering in $LuFe_2O_4$ [10] may be related to charge frustration.

The warwickite crystal structure of Fe_2OBO_3 (Fig. 1 inset) is prone to frustration, and we recently observed a CO superstructure with integer valence states (clearly distinct from a classical charge-density-wave) at low T [11]. Here, we present a detailed study of the thermal evolution of the CO in Fe_2OBO_3, establishing the presence of an unanticipated intermediate phase [12] with coexisting mobile and immobile carriers. Surprisingly, x-ray scattering indicates that the superstructure is incommensurate in the intermediate phase with a T dependent propagation vector $(\frac{1}{2}, 0, \tau)$. We show how the incommensuration arises from geometrical charge frustration via the proliferation of low-energy antiphase boundaries, as proposed also for *chemical order* in binary alloys [13]. Similar incommensurate phases may occur in other frustrated systems with "binary order" (e.g., Ising spins), and thus our results not only provide the first example of incommensurate phases with ionic (and therefore binary) CO, but have implications for

the broader study of geometrical frustration. In particular, we propose Fe_2OBO_3 as an ideal system to study ordering *dynamics* on frustrated lattices.

We studied single crystals from the same batch as those studied in [11]. The electrical resistivity was measured with standard four-probe geometry, using gold-sputtered contacts. Differential scanning calorimetry (DSC) was performed, with a Perkin-Elmer diamond DSC, on several powdered crystals, with temperature sweep rates between 10 and 50 K/min giving consistent results. The details of Mössbauer spectroscopy and electronic structure [generalized gradient approximation (GGA) + U] calculations are as in [11].

Synchrotron x-ray scattering was performed on two crystals with a mosaic spread of 0.20(8)° at the MU-CAT sector 6ID*B* of the Advanced Photon Source in the Argonne National Laboratory, with the photon energy tuned to 7.05 keV. All scattered intensities shown are normalized by an ion chamber monitor to account for changes in the incoming beam intensity. Because of the crystal mosaic spread and the presence of twinning, we determined the monoclinic distortion by rotating the crystal to the nominal (1, 3, 3) position and scanning the detector angle (similar to a powder diffraction experiment). Using the a, b, and c values obtained in [11] the monoclinic angle β was estimated, with error bars given by the uncertainty in a, b, and c. A further study was performed at 6ID*D* with photon energy $\sim$98 keV and an image plate system, using a rocking technique as in [14].

Between 250 and 400 K, resistivity $\rho(T)$ and DSC data [Figs. 1(a) and 1(b)] show two separate, well defined phase transitions on cooling (warming) at 340 and 280 (308) K, the former of which corresponds [Fig. 1(c)] to the monoclinic-orthorhombic structural transition. The transitions delineate low, intermediate, and high T phases. Ac
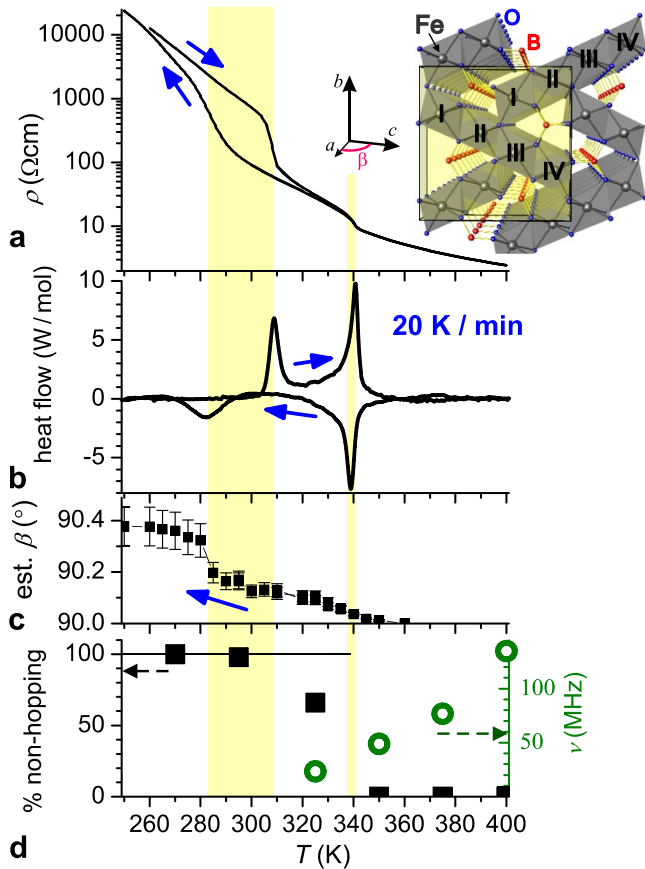
FIG. 1 (color online). Bulk physical properties of Fe_2OBO_3 indicating two phase transitions. (a)–(d) T dependence of resistivity ρ along a (a), heat flow of differential scanning calorimetry (b), estimated monoclinic angle β (c), and key parameters describing the Mössbauer spectra (d): fraction of the contribution to the spectra by Fe ions with no discernible electron hopping (■, left) and hopping frequency ν of the remainder (○, right). Inset in (a): Crystal structure at 355 K (after [11]).

specific heat had not revealed the lower transition [11], which we attribute to its insensitivity to irreversible contributions with hysteresis larger than the ac amplitude. In contrast, DSC is sensitive to *all* contributions to the specific heat. The estimated entropy change through both transitions [~ 0.6 J/(mol K) per Fe ion] still is only $\sim 10\%$ of the configurational entropy associated with perfect CO. Two likely reasons for this are discussed in what follows.

Mössbauer spectra (Fig. 2) indicate divalent and trivalent Fe ions distributed over two structural sites, as before [15]. However, whereas there is no discernible hopping of electrons between Fe ions at low T (hopping below ~ 1 MHz is not resolvable), the description of the high T spectra requires hopping with a T dependent frequency ν [Fig. 1(d), ○], which remains quite low even above 400 K [16]. In the intermediate T phase between the two transitions, e.g., at 325 K, contributions with and without electron hopping coexist [Fig. 1(d), ■]. Isomer shifts and
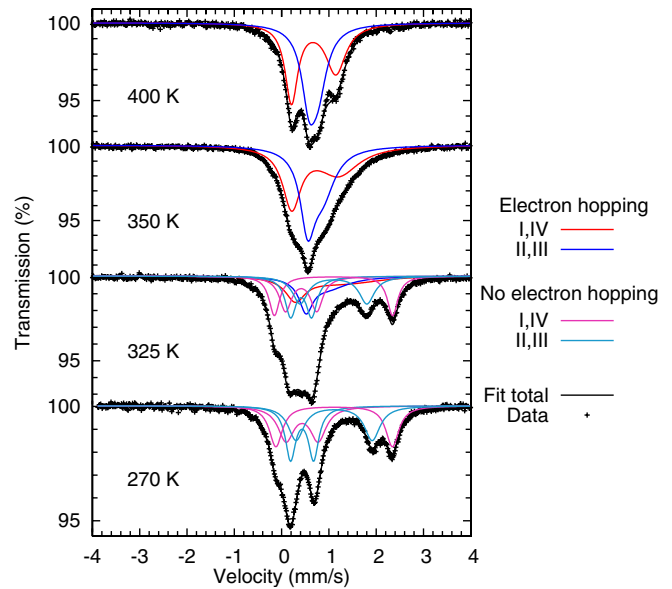

FIG. 2 (color online). Mössbauer spectra at selected T on powdered Fe_2OBO_3 crystals, modeled [16] with four contributions. At and below 325 K, the two nonelectron hopping doublets each for sites I, IV and II, III (labeled in the Fig. 1 inset) correspond to the two distinct Fe valences. Doublets with the larger (smaller) quadrupole splitting may be assigned to the site I, IV (II, III) [15]. The modeling indicates that the Fe^{2+} and Fe^{3+} quadrupole interactions have opposite sign for both the I, IV and the II, III site.

quadrupole splittings are equal for both contributions and follow a standard T dependence.

We further characterized the three phases by x-ray scattering using synchrotron radiation. In the low T phase, weak additional reflections [Fig. 3(a)] indexing to $(h + \frac{1}{2}, k, \ell)$ are observed, as expected [11]. Superstructure reflections are sharp along h and k. Along ℓ they are >25 times broader than fundamental reflections and indicate a correlation length, obtained by the inverse of the full width at half maximum, of only $\xi_c \sim 12c$. This suggests differently ordered domains [likely up and down diagonal CO [11]; see Fig. 4(a)] of size large along a and b, but small along c. These microdomains correspond to an imperfect overall CO, which is one reason for the lower-than-expected entropy. In the intermediate phase superstructure reflections are sharp along ℓ and are split, corresponding to an incommensurate modulation, with propagation vector $(\frac{1}{2}, 0, \tau)$, and $\tau(T)$ varying from about 0.4 at 340 K to 0.2 at 280 K [Fig. 3(b)]. Above 340 K a long-range ordered superstructure no longer exists, but very weak and broad reflections with $(h + \frac{1}{2}, k, \ell + \frac{1}{2})$ index [Fig. 3(d)] indicate persistent short-range correlated fluctuations, with correlations mainly along a, the chain direction. The correlations are not static, but the dynamics is relatively slow [Fig. 1(d)]. This dynamic short-range order likely also contributes to the "missing entropy." To test the incommensurability of the modulations in the intermediate tem-
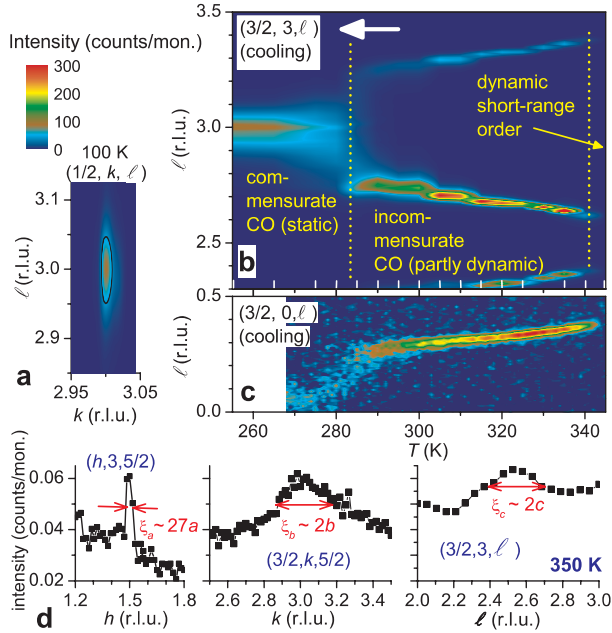
FIG. 3 (color online). Commensurate and incommensurate superstructure reflections from synchrotron x-ray scattering. Fundamental reflections at integers (h, k, ℓ) typically have peak intensities in excess of 10^4 counts/monitor. (a) Scattered intensity at $(\frac{1}{2}, k, \ell)$ and 100 K, showing one of the superstructure peaks corresponding to the doubled unit cell [11]. Black line: half-maximum-intensity contour. (b) Intensity at $(\frac{3}{2}, 3, \ell)$ vs T. An estimated beam heating of 5 K was corrected. Inner white ticks indicate T at which data were taken. (c) Intensity after background subtraction at $(\frac{3}{2}, 0, \ell)$ measured every 1 K in a different experimental setup with an image plate system. (d) h, k, and ℓ scans through $(\frac{3}{2}, 3, \frac{5}{2})$ at 350 K.

perature phase, data were collected in 1 K intervals with high-energy x rays. No indications for any "lock in" to commensurate values are visible in Fig. 3(c); thus the modulations are truly incommensurate rather than forming a devil's staircase as in [9].

To elucidate the microdomain formation at low T, and the incommensurate CO at intermediate T, we consider the energy of various CO configurations. The electrostatic energy is minimized by having as few same-valence nearest neighbors as possible. This requires strictly alternating valences along a within each chain and establishes "ordered chains" as the basic CO unit, consistent with the correlations in the fluctuation regime [Fig. 3(d)]. Geometrically, the 2D lattice of chains consists of two sublattices offset from each other by $\frac{a}{2}$ (1.6 Å): One sublattice comprises chains numbered I and III in Fig. 4 and in the inset of Fig. 1, the other chains II and IV. The electrostatic interactions between any two chains not belonging to the same sublattice are geometrically frustrated [Fig. 5(a)]. Therefore, flipping all valences in all chains (changing their phase) of one sublattice does not change the energy. Thus, the two configurations of Fig. 4(a) are degenerate in energy, as are the two of Fig. 4(b). This twofold degeneracy is lifted by a monoclinic distortion (ribbon tilting), and
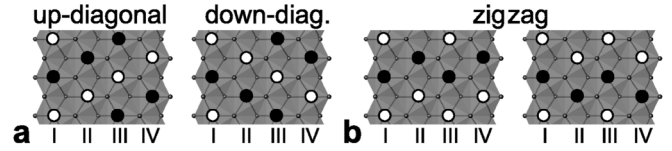

FIG. 4. Different charge order configurations within the four-chain ribbons of the Fe_2OBO_3 structure (Fig. 1 inset). Fe^{3+} (Fe^{2+}) are drawn as filled (open) circles. (a) Diagonal CO, the ground state. Degeneracy of the two configurations leads to domain formation, with opposite sense of monoclinic distortion [11]. (b) Alternative "zigzag" CO with only slightly higher energy than the diagonal ground state. All other configurations are intermediate between diagonal and zigzag.

hence the system will distort, thereby gaining energy [17]. However, according to our GGA + U calculations the energy gain associated with this distortion is very small, $\sim 0.2\%$ of the overall CO gain for diagonal CO [Fig. 4(a)], insufficient to prevent the facile formation of domains.

Neglecting the small monoclinic distortion there is no net interaction between the two sublattices so that further considerations can be restricted to one of them. Any two chains of the sublattice are either in-phase or antiphase [Fig. 5(b)] with a lower electrostatic energy if they are antiphase. Nevertheless, this does not remove all frustration because there is additional geometrical frustration even within one sublattice, due to the arrangement of chains projected in the bc plane [Fig. 5(c)]: Several "frustration triangles" are readily visible [highlighted in Fig. 5(c)]. Although this frustration is not exact (triangle sides have unequal length), various configurations are expected to be very close in energy. Indeed, while our GGA + U calculations established a diagonal CO [Fig. 4(a)] ground state [11], they also show that, e.g.,
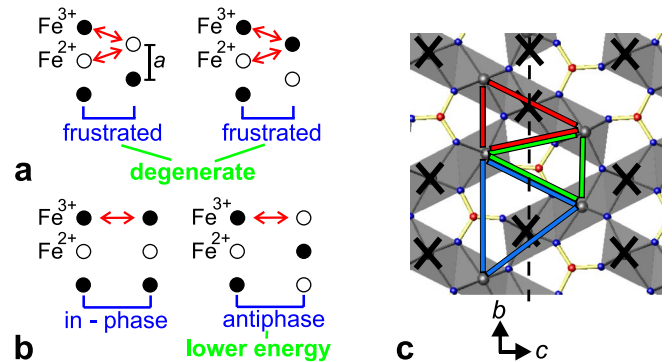

FIG. 5 (color online). Impact of geometrical frustration on the charge order. (a),(b) Phase relationship between two charge-ordered chains: For chains offset by $\frac{a}{2}$ (a), interchain electrostatic interactions are frustrated, and two configurations are degenerate in energy. Without offset (b), the antiphase configuration has lower energy. (c) bc projection of the Fe_2OBO_3 structure. The arrangement of chains leads to geometrical frustration even for interactions (thick lines) between chains with possible phase relationships as in (b) (the other chains are crossed out). Dashed line: possible antiphase boundary (see text).

the total energy gain due to zigzag CO [Fig. 4(b)] is only 1.9% [18] smaller than the one due to diagonal CO, despite having more chains in-phase rather than antiphase.

Because of this near degeneracy of configurations with different phase relationships, resulting from a hierarchy of geometrical frustration, the energy cost of creating an antiphase boundary in the *ab* plane [a possible location is indicated in Fig. 5(c)] between up and down diagonal CO domains [Fig. 4(a)] is small, explaining the small ξ_c. In contrast, there is no geometrical frustration within a chain, leading to a much larger ξ_a. ξ_b is large also due to the association of different CO domains with monoclinic distortions of opposite sense. A boundary in the *ac* plane between domains of different monoclinic angle β is not possible (short of cleaving the crystal), because the lattices will not match. In contrast, there is no problem matching domains with different β in *ab* or *bc* planes.

Incommensurate CO in classical charge-density-wave systems [6] and colossal magnetoresistance manganites [7] has been associated with Fermi-surface nesting. However, because Fe_2OBO_3 is far from metallic [Figs. 1(a) and 1(d)], a nesting scenario cannot account for the incommensurate modulations in the intermediate phase. A better analogy to our case of essentially perfect ionic CO is found in the *chemical* order of ions in binary alloys. In fcc-structured alloys, such as Cu-Au, incommensurate phases between chemically ordered (commensurate) and disordered phases are often observed and can be explained as a modulation with statistical period arising from antiphase boundaries easily created due to degeneracy and frustration of the bonds on triangular networks [13]. Given that in the intermediate phase of Fe_2OBO_3 the incommensurate modulation is in the *c* direction and the antiphase boundaries $\perp c$ are the ones with a small energy cost, we deduce that a similar scenario applies.

The strong and continuous *T* dependence of the propagation vector then implies that the boundaries move easily in the intermediate phase, and thermal excitations should cause them to fluctuate. Fluctuating boundaries reduce the monoclinic distortion [as observed, Fig. 1(c)] and they imply that a fraction of Fe ions, those near the boundaries, change their valences. Fe ions change their valence by electron hopping, providing a natural explanation for the presence, in the intermediate *T* phase, of both contributions with and without electron hopping in the Mössbauer spectra [Fig. 1(d)]. The coexistence of mobile and immobile electrons, reminiscent of nanoscale inhomogeneities prominent in manganites and cuprates [19], but coherently ordered in Fe_2OBO_3, further stabilizes the intermediate phase as a compromise between CO and delocalizing tendencies influenced by the geometrical frustration (without which the transition to a charge-ordered state likely would occur at much higher *T* [20]). Similar compromise phases may occur in other correlated electron systems with no chemical disorder.

In summary, we discovered an intermediate *T* phase of CO in Fe_2OBO_3, which is characterized by the coexistence of mobile and immobile carriers, and by an incommensurate superstructure, the latter of which can be explained by specific antiphase boundaries created easily due to geometrical charge frustration, similar to incommensurate *chemical* order. It should be interesting to further scrutinize the dynamics [5] of this model system of incommensuration from geometrical charge frustration.

*angst@ornl.gov

[1] G. Lawes *et al.*, Phys. Rev. Lett. **93**, 247201 (2004).
[2] R. Moessner and A. P. Ramirez, Phys. Today **59**, No. 2, 24 (2006).
[3] E. Wigner, Phys. Rev. **46**, 1002 (1934).
[4] E. J. W. Verwey, Nature (London) **144**, 327 (1939).
[5] H. Seo, K. Tsutsui, M. Ogata, and J. Merino, J. Phys. Soc. Jpn. **75**, 114707 (2006).
[6] G. Grüner, *Density Waves in Solids* (Perseus Publishing, Cambridge, MA, 1994).
[7] Y.-D. Chuang *et al.*, Science **292**, 1509 (2001); G. C. Milward, M. J. Calderon, and P. B. Littlewood, Nature (London) **433**, 607 (2005).
[8] P. G. Radaelli *et al.*, Nature (London) **416**, 155 (2002); Y. Horibe *et al.*, Phys. Rev. Lett. **96**, 086406 (2006).
[9] K. Ohwada *et al.*, Phys. Rev. Lett. **87**, 086402 (2001).
[10] N. Ikeda *et al.*, Nature (London) **436**, 1136 (2005).
[11] M. Angst *et al.*, Phys. Rev. Lett. **99**, 086403 (2007).
[12] An intermediate CO phase was reported in $TbFe_2O_5$ [P. Karen *et al.*, Phys. Rev. B **64**, 214405 (2001)], but no superstructure was observed in that phase.
[13] A. T. Paxton and H. M. Polatoglou, Phys. Rev. Lett. **78**, 270 (1997).
[14] A. Kreyssig *et al.*, Phys. Rev. B **76**, 054421 (2007).
[15] J. P. Attfield *et al.*, Nature (London) **396**, 655 (1998); A. P. Douvalis *et al.*, J. Phys. Condens. Matter **12**, 177 (2000).
[16] We employed the Blume-Tjon model [J. A. Tjon and M. Blume, Phys. Rev. **165**, 456 (1968)] for the analysis.
[17] Analogous to the Jahn-Teller effect [H. A. Jahn and E. Teller, Proc. R. Soc. A **161**, 220 (1937)].
[18] Even closer than in $LuFe_2O_4$ [H. J. Xiang and M.-H. Whangbo, Phys. Rev. Lett. **98**, 246403 (2007)].
[19] N. Mathur and P. Littlewood, Phys. Today **56**, No. 1, 25 (2003); E. Dagotto, Science **309**, 257 (2005).
[20] The activation energy in electrical transport corresponds to ~4000 K, setting an expected order of magnitude.